Antenna Miniaturization and Bandwidth Enhancement Using a Reactive Impedance Substrate

Hossein Mosallaei, *Senior Member, IEEE,* and Kamal Sarabandi, *Fellow, IEEE*

***Abstract*—The concept of a novel reactive impedance surface (RIS) as a substrate for planar antennas, that can miniaturize the size and significantly enhance both the bandwidth and the radiation characteristics of an antenna is introduced. Using the exact image formulation for the fields of elementary sources above impedance surfaces, it is shown that a purely reactive impedance plane with a specific surface reactance can minimize the interaction between the elementary source and its image in the RIS substrate. An RIS can be tuned anywhere between perfectly electric and magnetic conductor (PEC and PMC) surfaces offering a property to achieve the optimal bandwidth and miniaturization factor. It is demonstrated that RIS can provide performance superior to PMC when used as substrate for antennas. The RIS substrate is designed utilizing two-dimensional periodic printed metallic patches on a metal-backed high dielectric material. A simplified circuit model describing the physical phenomenon of the periodic surface is developed for simple analysis and design of the RIS substrate. Also a finite-difference time-domain (FDTD) full-wave analysis in conjunction with periodic boundary conditions and perfectly matched layer walls is applied to provide comprehensive study and analysis of complex antennas on such substrates. Examples of different planar antennas including dipole and patch antennas on RIS are considered, and their characteristics are compared with those obtained from the same antennas over PEC and PMC. The simulations compare very well with measured results obtained from a prototype $\lambda/10$ miniaturized patch antenna fabricated on an RIS substrate. This antenna shows measured relative bandwidth, gain, and radiation efficiency of $BW = 6.7\%$, $G = 4.5$ dBi, and $e_r = 90\%$, respectively, which constitutes the highest bandwidth, gain, and efficiency for such a small size thin planar antenna.**

***Index Terms*—Antenna miniaturization, finite-difference time-domain (FDTD), impedance surfaces, meta-substrates, perfectly magnetic conductor (PMC), periodic structures, planar antennas.**

I. Introduction

THE growing number of wireless applications has presented RF engineers with a continuing demand for low cost, power efficient, and small-size system designs. Depending on the application at hand and required system characteristics, such as data-rate, environment, range, etc., the system parameters such as operating frequency, transmitter power, and modulation scheme may vary widely. However, independent of the application, compactness, wide bandwidth, high efficiency, ease of fabrication and integration, and low cost are always sought in wireless systems.

One of the most important components of wireless systems is their antenna. Planar antennas, because of their ease of fabrication/integration as well as compactness and low-profile characteristics, are highly desirable for these systems. The substrates of planar antennas play a very important role in achieving desirable electrical and physical characteristics. Planar antennas are usually considered for applications where the antenna is to be mounted on a platform. In these situations, a significant front-to-back radiation ratio is desired to minimize the influence of the platform on the antenna input impedance and radiation characteristics. Design of antenna elements with significant front-to-back radiation ratio is either accomplished through the use of metal-backed substrates or high dielectric superstrates [1]–[3]. Dielectric resonator antennas [4], [5] belong to the latter class, which show relatively high bandwidth and efficiency for a specified compact antenna size. However, these types of antennas are not low-cost nor are they easily integrated with the rest of RF electronics. In addition, antennas using dielectric (or magnetodielectric) superstrates can be heavy and somewhat bulky. On the other hand printed antennas on metal-backed substrates have limited bandwidth and efficiency. This problem stems from the fact that the radiated field from the image of the antenna's electric current, which is placed in close proximity and parallel to a perfectly electric conductor (PEC), tends to cancel out the radiated field from the antenna current itself. In this case matching the antenna input impedance is rather difficult, and if a matching condition can be achieved, it would be over a relatively narrow bandwidth. This effect results from significant increases in the stored electromagnetic energy of the antenna near-field due to the presence of PEC ground plane. This in turn increases the antenna radiation Q, or equivalently decreases the antenna bandwidth.

To circumvent this difficulty, considerable efforts have been devoted in recent years toward the development of high impedance surfaces or artificial perfectly magnetic conductors (PMC) [6], [7]. Basically PMC surfaces provide the desired front-to-back radiation ratio and allows for the placement of parallel electric currents in their close proximity. The image of parallel electric current in PMC surface is in-phase and parallel to the original current distribution. Hence the radiated fields add up in-phase, and the antenna impedance matching appears to be easier. In this case, the input resistance is doubled, which is not a serious problem, but matching the reactive part is still difficult. As is the case for PEC ground planes, the stored EM energy in the near field is increased considerably. The most important drawback of PMC surfaces is

Manuscript received May 29, 2003; revised November 3, 2003. This work was supported by the Defense Advanced Research Projects Agency (DARPA) under Contract N000173-01-1-G910.

The authors are with the Department of Electrical Engineering and Computer Science, University of Michigan-Ann Arbor, Ann Arbor, MI 48109-2122 USA (e-mail: hosseinm@engin.umich.edu).

Digital Object Identifier 10.1109/TAP.2004.834135

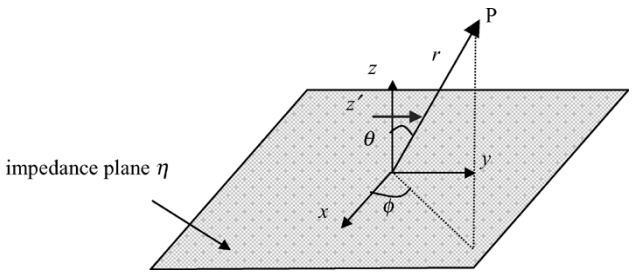

Fig. 1. Geometry of infinitesimal dipole Il in y direction located at z' above the impedance plane η.

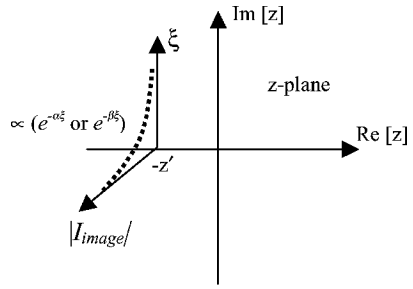

Fig. 2. Distributed image source in complex z-plane along the $-z' + j\xi$ line. The current distribution is decayed with the $e^{-\alpha\xi}$ & $e^{-\beta\xi}$ factors. Notice that for the dipole located above the reactive surface the image current has the sinusoidal distribution.

the low overall antenna efficiency. PMC surfaces are usually constructed from resonant structures operating at resonance. In practice, where there are finite dielectric and conductor losses PMC surfaces become lossy and absorb the antenna near-field energy. This results in low overall antenna efficiency.

Hence, the antenna substrate is a key component, affecting all aspects of the antenna radiation and input impedance characteristics. It appears that, with few exceptions, all functionalities offered by an antenna substrate have not been fully exploited. The main objective of this paper is to investigate other substrate design possibilities and examine the advantages and improved functionalities offered by them. In specific this paper presents the theory, design, and fabrication of a class of reactive impedance surface (RIS) substrates. The objectives in such design process are to minimize the adverse effects of the antenna interaction with the substrate such as the mutual coupling between the antenna and its image, and accentuate positive interactions such as an appropriate spectral trend of stored electric and magnetic energy which can result in enhanced bandwidth and/or antenna miniaturization.

In what follows first the basic concept of RIS substrates is introduced, then the performance of an ordinary half-wave dipole in free-space, over a PEC ground plane, and over a PMC ground plane are presented and compared. In Section IV a specific RIS substrate design is presented and the analytical formulation and numerical simulations for such design are provided. Finally performance of planar antennas on this RIS substrate is demonstrated through simulations and measurements.

II. The Basic Concept

As explained above, both PEC and PMC surfaces have a strong coupling with the antennas above them and neither is appropriate as the ground plane for antenna designs. In order to alleviate the adverse effects of the standard ground planes, an impenetrable surface that minimizes the coupling effect is needed. Recent works on speeding up calculation of Sommerfeld type integrals has led to derivation of fast converging integrands that attribute the field of a dipole above half-space to a distributed image current in a complex domain [8]–[10]. It turns out that the expressions for the image current distribution can be obtained in a close form for impedance surfaces [11], [12]. Since the image current is distributed in space for impedance surfaces, it is expected that the effect of the mutual coupling would be smaller. To further examine this point let us consider a horizontal (y-directed) infinitesimal electric current above an impedance surface with impedance η. Fig. 1 shows the geometry of the problem where the current filament with a dipole moment Il is placed at a height z' above the impedance plane.

Expanding the dipole field in terms of a continuous spectrum of plane waves and imposing the impedance boundary condition $\hat{\mathbf{n}} \times (\hat{\mathbf{n}} \times \mathbf{E}) = -\eta(\hat{\mathbf{n}} \times \mathbf{H})$ one can determine the Hertzian vector potential Π [12] as

$$\Pi = \hat{y}\Pi_y + \hat{z}\Pi_z = -\frac{j\eta_0 Il}{4\pi k_0}\left[\hat{y}\left(\frac{e^{-jk_0R_1}}{R_1} + \left(\frac{e^{-jk_0R_2}}{R_2} - 2\alpha\int_0^\infty e^{-\alpha\xi}\frac{e^{-jk_0R_2'(\xi)}}{R_2'(\xi)}d\xi\right)\right) - \hat{z}\frac{2}{k_0}\frac{\frac{\eta}{\eta_0}}{1-\left(\frac{\eta}{\eta_0}\right)^2}\frac{\partial^2}{\partial y\partial z}\int_0^\infty\left(e^{-\alpha\xi}-e^{-\beta\xi}\right)\frac{e^{-jk_0R_2'(\xi)}}{R_2'(\xi)}d\xi\right] \tag{1}$$

where

$$R_1 = \sqrt{x^2+y^2+(z-z')^2} \tag{2a}$$

$$R_2 = \sqrt{x^2+y^2+(z+z')^2} \tag{2b}$$

$$R_2'(\xi) = \sqrt{x^2+y^2+(z+z'-j\xi)^2} \tag{2c}$$

$$\alpha = \frac{\eta_0 k_0}{\eta}, \quad \beta = \frac{\eta k_0}{\eta_0}. \tag{2d}$$

For the special cases of PEC (zero impedance) and PMC (infinite impedance) (1) is reduced to

$$\text{PEC Surface}: \Pi = -\hat{y}\frac{j\eta_0 Il}{4\pi k_0}\left(\frac{e^{-jk_0R_1}}{R_1} - \frac{e^{-jk_0R_2}}{R_2}\right) \tag{3a}$$

$$\text{PMC Surface}: \Pi = -\hat{y}\frac{j\eta_0 Il}{4\pi k_0}\left(\frac{e^{-jk_0R_1}}{R_1} + \frac{e^{-jk_0R_2}}{R_2}\right). \tag{3b}$$

The first and second terms in the parenthesis represent the contributions of the dipole located at z' and its image at $-z'$, respectively.

In general, for an arbitrary impedance surface η, (1) can be interpreted as the vector potential of the dipole in position z' and a distributed linear image source in the complex z-plane along the $-z' + j\xi$ line as illustrated in Fig. 2. The image current has exponentially decaying ($e^{-\alpha\xi}$ and $e^{-\beta\xi}$) distribution. For surfaces with real impedance values, the image current is

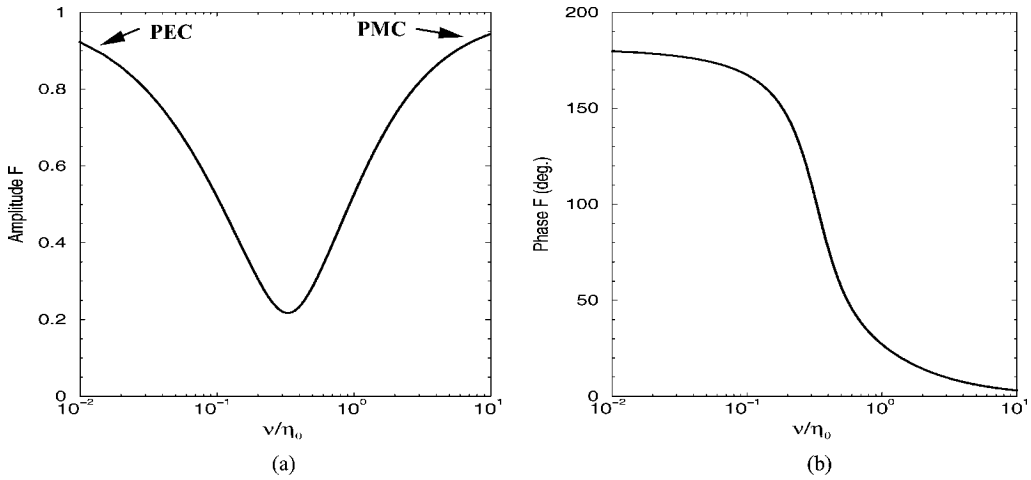

Fig. 3. Effect of image source in the reactive impedance plane ($\eta = j\nu$) at the source location [mutual coupling-$F(\nu/\eta_0)$]. (a) Amplitude and (b) phase. Notice that the PEC and PMC surfaces produce the maximum image contributions and the minimum coupling occurs at $\nu/\eta_0 = 0.33$.

mostly concentrated at image point $-z'$, similar to the conventional PEC and PMC surfaces, and therefore mutual coupling is expected to be high. However, for a purely reactive impedance plane with moderate value of $\eta = j\nu$ the image current has a sinusoidal form and instead of being focused at point $-z'$ (close to the source), it is distributed along the line $-z' + j\xi$, and therefore has a markedly reduced mutual interaction with the source itself. That is; the field of the dipole image at the source point itself can be minimized by a proper choice of impedance value. This behavior suggests that placing antennas over reactive impedance surfaces can provide a significantly wider bandwidth. Fig. 3 shows the effect of a dipole image in a reactive impedance plane, at the source location ($z' = 0.02\lambda_0$), as a function of normalized impedance ν/η_0. This effect is shown by plotting

$$F\left(\frac{\nu}{\eta_0}\right) = \left.\frac{\frac{e^{-jk_0R_2}}{R_2} - 2\alpha\int_0^\infty e^{-\alpha\xi}\frac{e^{-jk_0R_2'(\xi)}}{R_2'(\xi)}d\xi}{\frac{e^{-jk_0R_2}}{R_2}}\right|_{(0,0,z')} \tag{4}$$

which represents the ratio of image contribution of a dipole over an RIS to that over a PEC or PMC, as a function of ν/η_0. Noting that $\partial R_2'(\xi)/\partial y|_{(0,0,z')} = 0$, the z-component of Π vanishes at the source location. As clearly demonstrated in Fig. 3, the image contribution at the source point (mutual coupling) is maximum for PEC and PMC surfaces and is reduced by -14 dB for a certain value of surface reactance (in this case $\nu/\eta_0 = 0.33$).

It is also important to note that the plane wave reflection coefficient of impedance surfaces given by

$$\Gamma = \frac{\eta\cos\theta - \eta_0}{\eta\cos\theta + \eta_0} \tag{5}$$

has a magnitude of unity and a phase ϕ that varies between 180° and $-180°$ for surfaces with purely reactive impedance values. Using plane wave expansion for any arbitrary source excitation above an RIS, and noting the reflection coefficient for each plane wave has a unity magnitude, total power refection is ensured. In addition the normalized impedance can be chosen so that the stored energy in the image source could compensate for the energy stored by the source itself. That is; if the antenna shows a capacitive load and its image can store magnetic energy, a resonance can be achieved at a frequency much lower than the resonant frequency of the antenna in free space. These novel features are successfully highlighted in the following sections.

III. Analysis of Dipole Antennas in Free Space and Over PEC and PMC Ground Planes

In this section the performance analysis of dipole antenna over PEC and PMC ground planes is presented, and the adverse effects of these surfaces are quantitatively illustrated. An advanced FDTD computational engine, developed at UCLA, is employed in these analyzes [13]–[15]. In specific a half-wave dipole in free space and over the finite-size PEC and PMC ground planes is considered and analyzed.

A. Antenna in Free Space

To establish a reference we first consider a dipole in free space. Fig. 4(a) depicts the geometry of a dipole antenna with length 6.30 cm and diameter-to-length ratio of about 0.01. The dipole is excited using a probe feed from the middle. The input resistance and reactance of antenna ($Z_a = R_a + jX_a$) are computed using the FDTD method and plotted in Fig. 5. The dipole is matched at frequency $f_0 = 2.11$ GHz (see Fig. 6) at which frequency its length is $0.45\lambda_0$. Fig. 6 shows that the half-wave dipole antenna can be simply matched to a 50 Ω line with a 10 *dB* bandwidth of $BW = 9.71\%$.

B. Dipole Over a Finite-Size PEC Ground Plane

The geometry of a dipole antenna over a finite PEC ground plane with dimensions 10.80 cm $\times$ 10.80 cm is shown in Fig. 4(b). The FDTD is applied to analyze the behavior of the dipole over the finite-size PEC, and the results for the input impedance are presented in Fig. 7(a). The PEC remarkably changes the impedance performance of antenna. The minimum return loss occurs at $f_0 = 2.18$ GHz, as shown in Fig. 6. However, impedance matching with the use of an external matching network cannot be accomplished due to extremely low input resistance. The antenna radiation patterns at $f_0 = 2.18$ GHz with a ground plane size $0.78\lambda_0 \times 0.78\lambda_0$ are plotted in

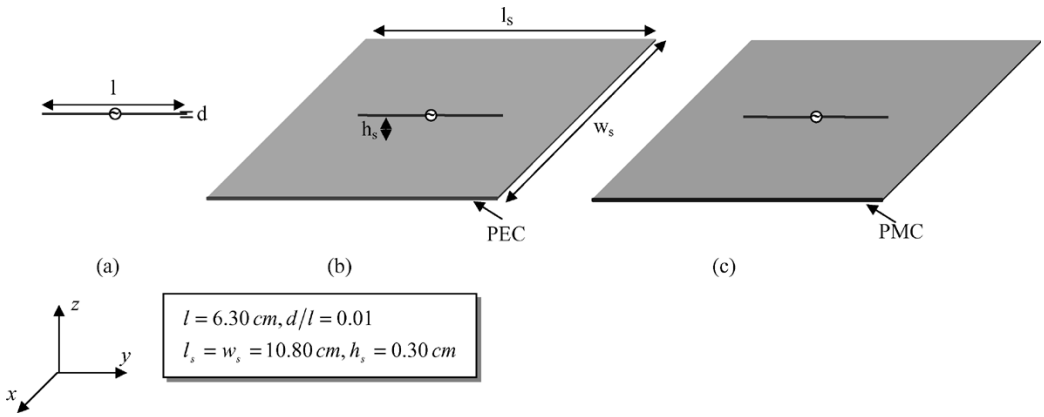

Fig. 4. Dipole antenna in (a) free space and over the (b) PEC and (c) PMC surfaces. Dipole is excited in the middle utilizing probe feed.

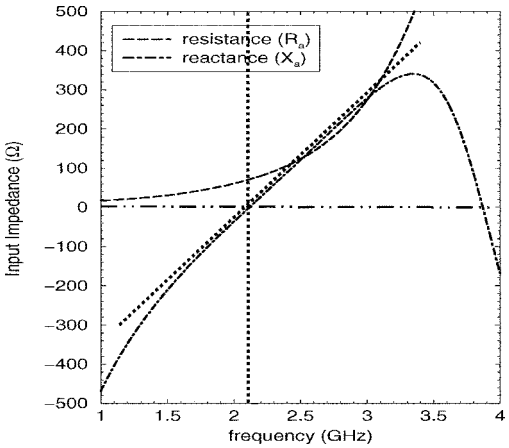

Fig. 5. Input impedance of dipole antenna in free space.

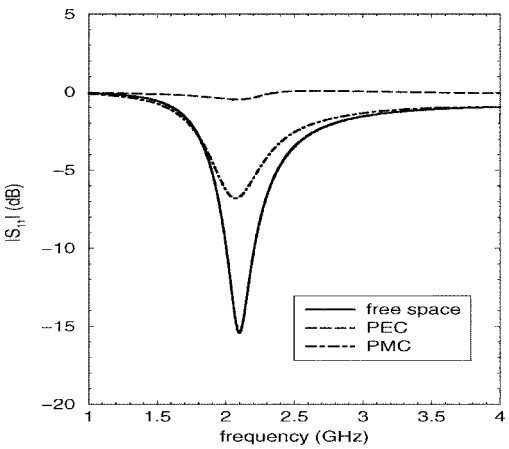

Fig. 6. Return loss of dipole antenna in free space and over the PEC and PMC surfaces. Notice that the dipole close and parallel to the PEC and PMC planes cannot be matched.

Fig. 7(b). The directivity and front-to-back ratio are calculated to be $D_0 = 8.78$ dB and 17 dB, respectively.

C. Finite-Size PMC Ground Plane

The performance of a dipole antenna above an ideal PMC ground plane [Fig. 4(c)] is presented here. Similar to the PEC ground plane, there exists a strong coupling between the PMC surface and the antenna above it; however, in this case the image current is in-phase and parallel to the dipole source. The FDTD results for the input impedance of a dipole above a finite-size ideal PMC are shown in Fig. 8(a). Compared to the dipole in free-space, the input resistance is almost doubled, and the slope of the reactance versus frequency is increased. Although performance of the antenna over PMC is much better than the antenna over PEC, the input impedance could not be directly matched as shown in Fig. 6. As mentioned earlier the reactance slope is increased and therefore even if the antenna can be matched using an external matching network, the bandwidth would be lower than the free-space case. This clearly demonstrates that the PMC surface is not a proper choice for the antenna ground plane as was suggested in [6]. Choosing the operating frequency at the minimum of return loss ($f_0 = 2.12$ GHz), the directivity and front-to-back ratio are found to be $D_0 = 6.75$ dB and 14 dB, respectively [shown in Fig. 8(b)].

IV. RISs

The previous sections discussed the drawbacks of antennas designed over PEC and PMC ground planes. It was also postulated that using a RIS with surface impedance $\eta = j\nu$, antenna impedance matching and bandwidth enhancement could be achieved. In addition, it was mentioned that antenna miniaturization could be accomplished by the proper choice of surface reactance. In this section, first a practical approach for designing arbitrary reactive impedance surfaces is presented and then performances of different antennas on such surfaces are examined.

A. Practical Design of RISs

The objective here is to demonstrate a method for designing a reactive surface with a prescribed surface impedance property. To accomplish this, an RIS structure composed of a periodic array of square patches printed on a PEC-backed dielectric substrate with thickness d and permittivity ε_r is introduced. To distinguish the structure from the frequency selective surfaces (FSS) it should be emphasized that the periodicity of the RIS metallic patches is much smaller than the wavelength.

In order to facilitate the design procedure, a simple and yet very accurate circuit model for the structure is developed. Accuracy of this model is verified using the FDTD technique in

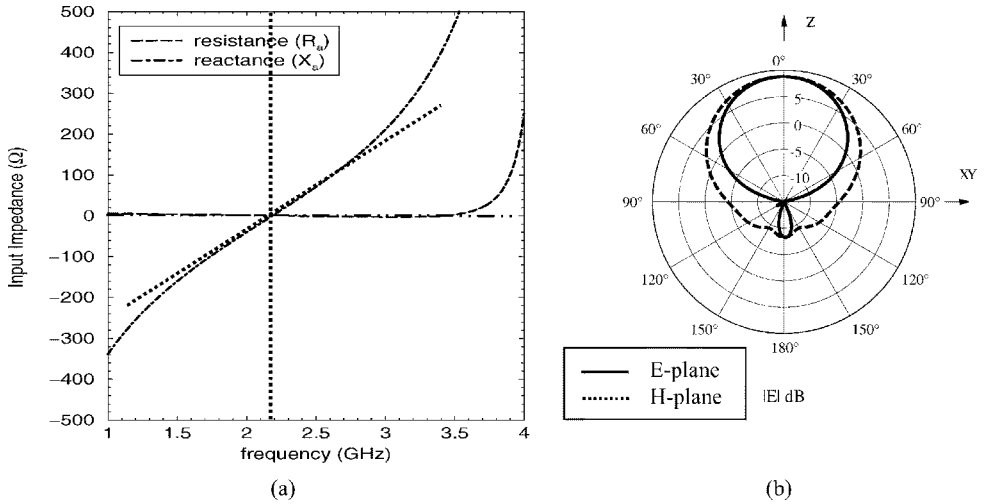

Fig. 7. Performance of dipole antenna over the PEC plane, (a) Input impedance, (b) Radiation patterns. Notice that the input resistance is almost zero and its reactance has a smother slope in compared to the dipole in free space. PEC reduces the back radiation.

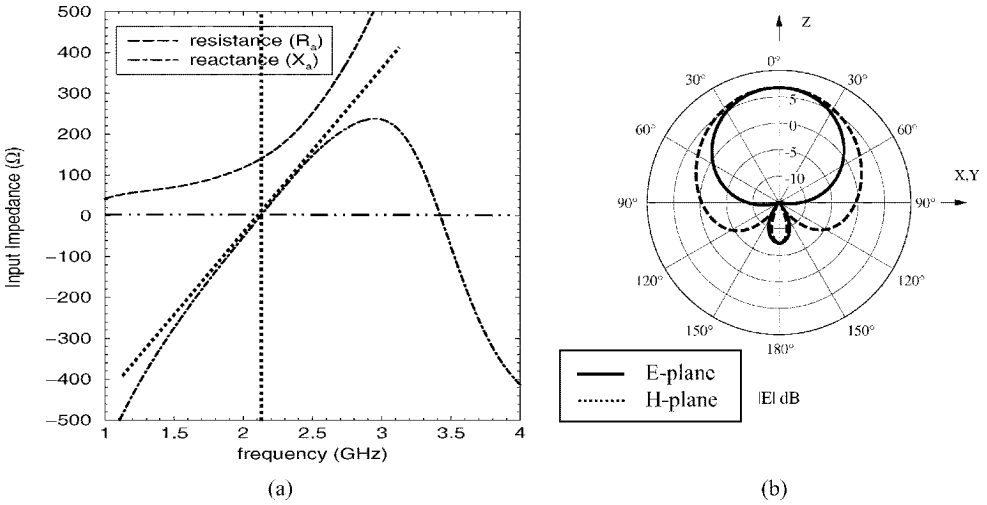

Fig. 8. Performance of dipole antenna over the PMC plane: (a) input impedance and (b) radiation patterns. Notice that compared to the dipole in free space the input resistance is almost doubled and its reactance is enhanced. PMC reduces the back radiation.

conjunction with periodic boundary conditions (PBC) and perfectly matched layer (PML) walls [14], [15]. The FDTD is also used to analyze the behavior of different antennas on such surfaces.

The geometry of the proposed RIS is shown in Fig. 9. We first consider the interaction of this structure with a normal incidence plane wave. In this case it turns out that only a single cell can be considered in the analysis by establishing PEC and PMC plates around the cell perpendicular to the incident electric field and magnetic field. The resulting structure can be modeled using a transmission line as shown in Fig. 10. The square patch acts as a shunt capacitor placed at a distance d from a short-circuited dielectric loaded transmission line. This short-circuited dielectric loaded transmission line can be modeled by a lumped shunt inductor parallel to the capacitor. Now it is clear that this structure, depending upon the values of the capacitance, inductance, and operating frequency, can behave as a capacitive or inductive RIS. The parallel LC circuit is inductive at frequencies below resonance, open circuit at the resonance (behaving as a PMC surface) and capacitive above the resonant frequency. At frequencies much lower than the resonant frequency the surface impedance approaches zero and the structure behaves as a PEC surface. The impedance ($\eta = j\nu$) of the surface can simply be obtained from

$$\eta = Z_{LC} = j\frac{X_L X_C}{X_C - X_L} = jX_{LC} \tag{6}$$

where

$$X_L = Z_d \tan kd \tag{7a}$$

$$k = k_0\sqrt{\varepsilon_r} \tag{7b}$$

$$Z_d = \frac{\eta_0}{\sqrt{\varepsilon_r}} \tag{7c}$$

$$X_c = \frac{1}{\omega C}. \tag{7d}$$

An approximate expression for the coupling capacitance C can be obtained using the closed form equation for the capacitance

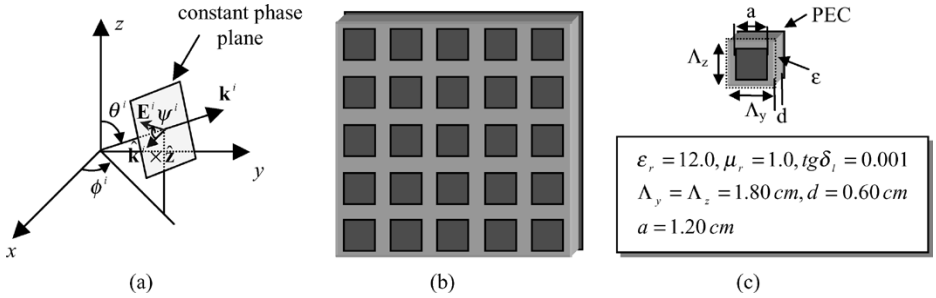

Fig. 9. RIS substrate composed of periodic squared patches printed on the PEC-backed dielectric material. (a) Plane wave illumination and its corresponding coordinate system, (b) periodic structure and its (c) building block unit cell.

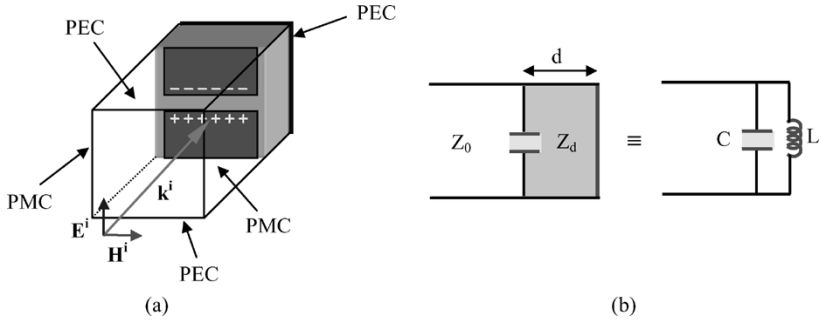

Fig. 10. Circuit approach representation of the RIS medium. (a) Unit cell of RIS bounded to the PMC-PEC walls in the y-z directions and illuminated by the normal incident plane wave. (b) Parallel LC equivalent model. Notice that the backside PEC after the distance d presents the inductive property.

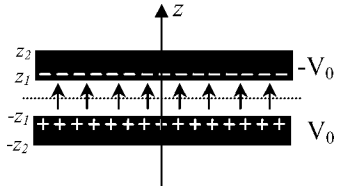

Fig. 11. Coplanar strips at potential $\pm V_0$ and location $z_1 \leq |z| \leq z_2$ (infinite length). The existence capacitor per unit length between the strips is denoted C_0 and determined using (8).

per unit length of two coplanar strips, as shown in Fig. 11, given by [16], [17]

$$C_0 = \frac{\varepsilon K\left(\sqrt{1-\left(\frac{z_1}{z_2}\right)^2}\right)}{K\left(\frac{z_1}{z_2}\right)} \tag{8}$$

where $K(z)$ is the complete elliptic integral defined by

$$K(z) = \int_0^{\pi/2} \frac{d\phi}{\sqrt{(1-z^2\sin^2\phi)}} = \frac{\pi}{2}\left(1+\frac{1^2}{2^2}z^2+\frac{1^2\cdot 3^2}{2^2\cdot 4^2}z^4+\frac{1^2\cdot 3^2\cdot 5^2}{2^2\cdot 4^2\cdot 6^2}z^6+\cdots\right) \quad [z^2<1] \tag{9}$$

and z_1, z_2, as shown in Fig. 11, define the vertical coordinates of the strip edges. The capacitance C is obtained by multiplying C_0 with the effective length ($\widetilde{a}$) of the square patch (slightly shorter than its physical length because of the finite size edge effects).

The formulation obtained so far is valid for normal incidence plane waves. Next, we show how this formulation [(6)] can be extended to oblique incidence plane waves with arbitrary polarization. Noting the symmetry of square patches, this can be done rather easily by replacing X_L with $X_{L,\mathrm{TE}}$ and $X_{L,\mathrm{TM}}$ given by

$$X_{L,\mathrm{TE}} = \left(\frac{Z_d}{\cos\alpha}\right)\tan\left(kd\cos\alpha\right) \tag{10a}$$

$$X_{L,\mathrm{TM}} = \left(Z_d\cos\alpha\right)\tan\left(kd\cos\alpha\right). \tag{10b}$$

Here, TE and TM denote the wave polarization state with respect to the plane of incidence defined by the propagation vector and normal to the surface; and α is the angle of transmission (inside the dielectric material) measured from the normal direction.

As an example, let us consider a composite medium of periodic square patches with patch dimensions 1.20 cm × 1.20 cm and periodicity $\Lambda_y = \Lambda_z = 1.80$ cm printed on a dielectric material with relative permittivity $\varepsilon_r = 12.0$, and thickness $d = 0.60$ cm backed by a PEC surface. To characterize the electromagnetic behavior of this surface, the approximate circuit model and the FDTD technique are used. In this case, the gap between patches is 0.6 cm, which corresponds to $z_1/z_2 = 1/3$. Using (8) for the finite size patch with an effective length $\widetilde{a} < a$, and assuming that half of the field is in air and the other half is in the dielectric, the capacitance C can be calculated from

$$C \approx \frac{\varepsilon K\left(\sqrt{\frac{8}{9}}\right)}{K\left(\frac{1}{3}\right)}\cdot\widetilde{a} \approx 0.0138\varepsilon_0\frac{\varepsilon_r+1}{2} = 0.79\,pf. \tag{11}$$

Equations (6) and (7), are then used to evaluate the approximate surface impedance η. The normalized surface reactance ν/η_0 of the proposed composite medium as a function of frequency is plotted in Fig. 12(a). As mentioned before at low frequencies the RIS shows low impedance and acts as a PEC surface and at the resonance the reactance goes to infinity and the RIS

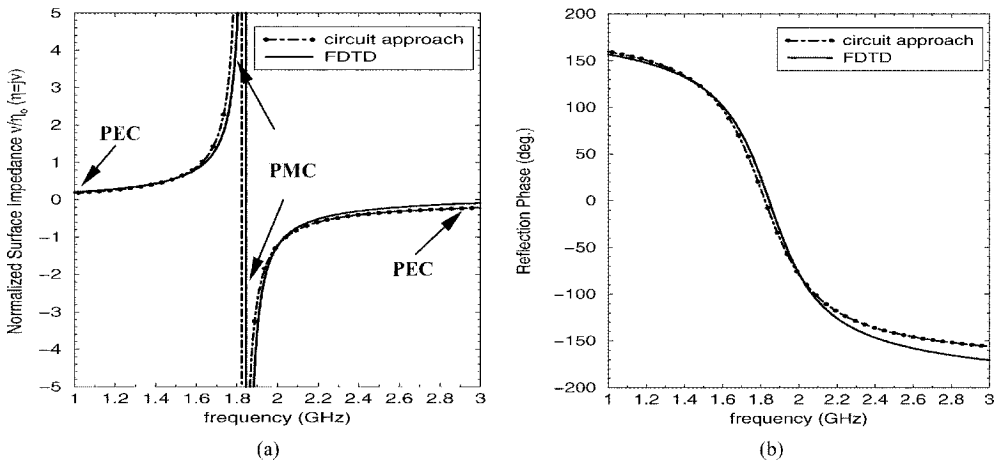

Fig. 12. Characteristics of the RIS substrate for the normal incident plane wave determined utilizing the circuit approach and FDTD technique. (a) Normalized surface impedance and (b) reflection phase. Notice to the novel surface performance lying between the PEC and PMC planes. An excellent agreement between the analytical and numerical methods is observed.

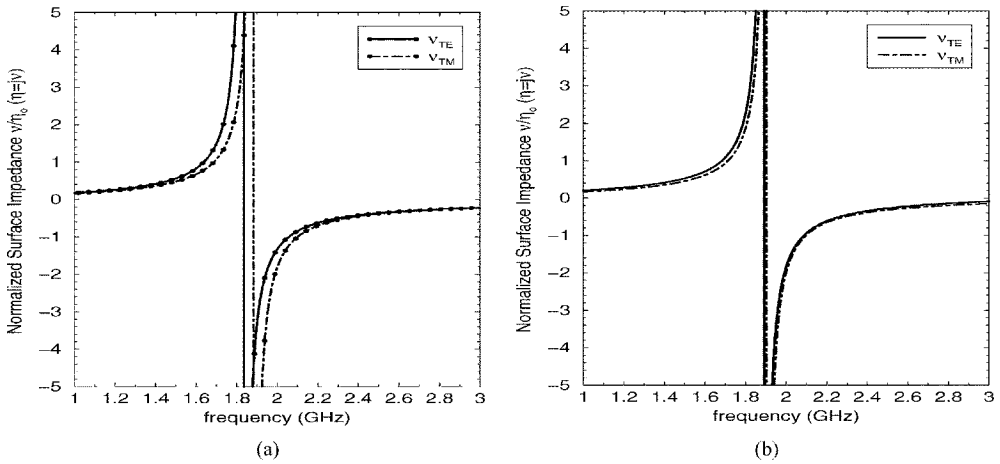

Fig. 13. Oblique incident surface impedance performance of the RIS substrate for arbitrary plane wave $\theta^i = 90°$, $\theta^i = 120°$, $\psi^i = 50°$ [coordinate system is defined in Fig. 9(a)]. (a) Circuit model approach and (b) FDTD technique. Comparing to Fig. 12, the surface reactance is almost independent of polarization and incidence angle.

behaves as a PMC. In this plot the surface impedance obtained from FDTD simulation (see [15]) is also displayed where excellent agreement between the FDTD and analytical formulation is observed. The phase of reflection coefficient Γ of the RIS using

$$\Gamma = \frac{\eta - \eta_0}{\eta + \eta_0} = \frac{j\nu - \eta_0}{j\nu + \eta_0} = e^{j\phi} \tag{12}$$

and the FDTD results are shown in Fig. 12(b) and again an excellent agreement is obtained.

Next consider simulation of surface impedance of the structure as seen by an oblique incidence and arbitrary polarization plane wave. Fig. 13 shows the surface reactance of the RIS at an incidence angle 60°($\theta^{\mathrm{i}} = 90°$, $\phi^{\mathrm{i}} = 120°$) with a linear polarization specified by angle $\psi^{\mathrm{i}} = 50°$ (between the electric field and a reference direction $\hat{\mathbf{k}}^{\mathrm{i}} \times \hat{\mathbf{z}}$). The results are determined utilizing both the circuit model and the FDTD techniques and shown in Fig. 13 with very good agreement.

Due to the symmetric shape of periodic patches the performance of RIS is almost independent of the polarization states (in x-y plane). Additionally, if a relatively large dielectric constant is used, according to Snell's law, $\cos\alpha$ remains close to unity independent of incidence angle in free space. Therefore surface reactance of the RIS becomes invariant to incidence angle and polarization as desired.

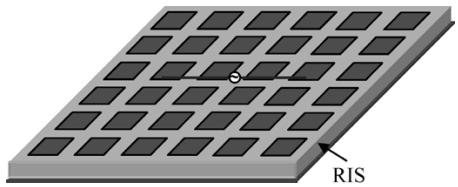

Fig. 14. Dipole antenna over the RIS substrate. RIS is a 6×6 finite array of square patches printed on the PEC-backed dielectric material.

Note that, in contrast to the Sievenpiper's mushroom surface [6], no type of via-hole is used in the designed RIS here.

B. Antennas Over Reactive Impedance Surfaces

In the previous section, a practical method for designing an RIS with desired parameters was presented. Although the periodic composite surface is only an approximate rendition of a mathematical impedance surface, its interaction with EM waves should produce the desired results. As mention earlier, design of planar antennas over RIS has a number of advantages including wider bandwidth and size reduction while providing the

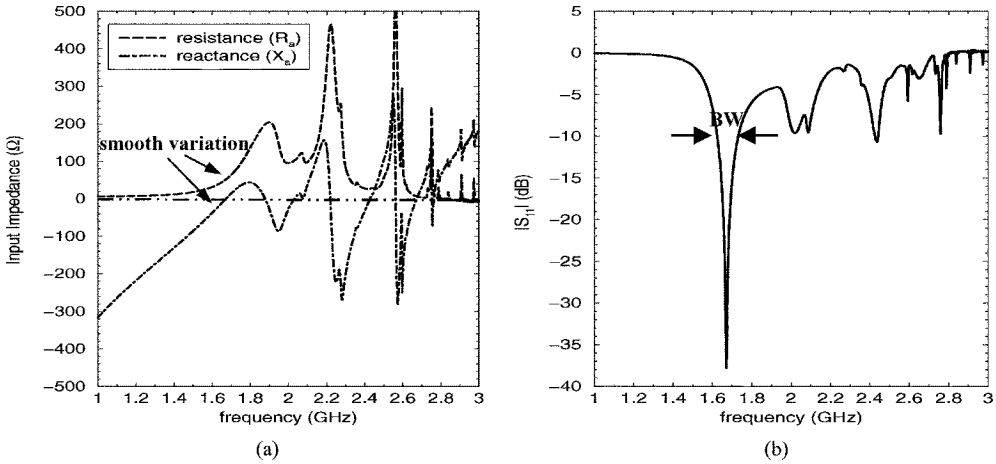

Fig. 15. Input impedance of dipole antenna over the RIS substrate: (a) Input resistance and reactance and (b) return loss. The RIS provides a miniaturized size and wide bandwidth.

desired front-to-back ratio. In the present section, these features are examined by demonstrating the performance of a dipole and a patch antenna over a RIS.

1) Dipole Over RIS: The geometry of a dipole antenna above the finite-size RIS designed in the previous section is shown in Fig. 14. The finite-size RIS is composed of a 6×6 array of square patches whose dimensions are provided in Fig. 9(c). The dipole antenna has the same dimensions as those studied in the previous examples with a free-space operating frequency of $f_0 = 2.11$ GHz. The input impedance and the radiation patterns of the antenna are obtained using the FDTD full-wave simulation tool and are shown in Figs. 15 and 16, respectively. As demonstrated in Fig. 12, the RIS has a resonant frequency of $f_{\rm RIS} = 1.84$ GHz at which it acts like a PMC. Below this resonance the RIS is inductive. Also as seen in Fig. 5, the dipole is capacitive below 1.84 GHz. The ability of the surface to store magnetic energy compensates for the electric stored energy in the near-field of the dipole below its natural resonant frequency. This results in antenna miniaturization. As shown in Fig. 15 the operating frequency (zero crossing of antenna input reactance) of the dipole over the RIS is at $f_0 = 1.67$ GHz substantially below the free-space operating frequency 2.11 GHz. At this frequency the dipole length is $0.35\lambda_0$. Also comparing the slope of the antenna input reactance to that of the dipole over PEC or PMC, it is clear that a much wider bandwidth can be achieved. Fig. 15(b) shows the return loss of the dipole over the RIS with a high relative bandwidth of 6.40%. Considering the size reduction of 30%, the antenna relative bandwidth is comparable to that of the dipole in free-space (10%). Referring to Fig. 16, the radiation pattern of the dipole over RIS shows a remarkable front-to-back ratio of 20 dB. Simulation results also show a directivity of about 6.70 dB and a high radiation efficiency of $e_r = 96\%$.

It is also obtained from Fig. 15 that the return loss has a null at the RIS resonance frequency where the surface behaves as a PMC. At this frequency the resonant surface becomes purely resistive (material loss) and dissipates the antenna input power. Since all dielectric materials have some finite loss tangent, this power dissipation represents another draw back of using PMC as a substrate for planar antennas. Fig. 17 shows the absorption rate of the RIS for a normal incident plane wave for different

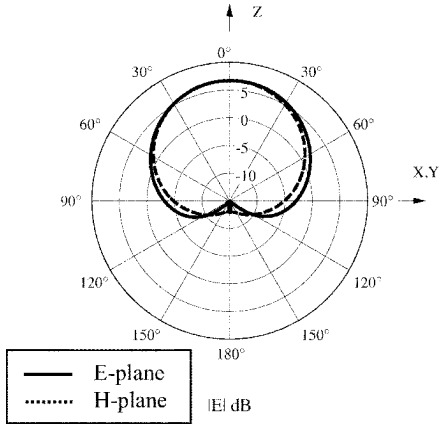

Fig. 16. Radiation patterns of dipole antenna over the RIS substrate. The back radiation is remarkably reduced.

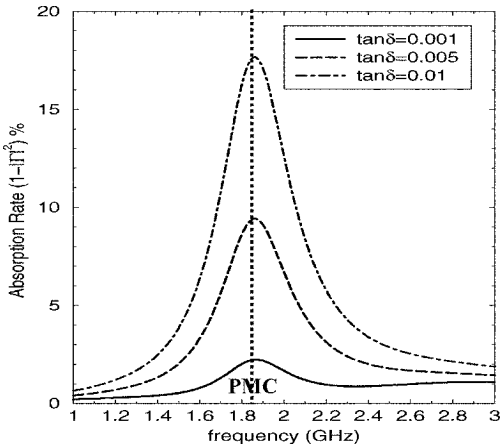

Fig. 17. Absorption rate of the RIS for a normal incident plane wave. Notice to the lossy behavior of RIS at the resonance (PMC surface).

loss tangents $\tan\delta = 0.001$, 0.005, and 0.01. It clearly demonstrates the lossy behavior of RIS at resonance (PMC surface). The calculated radiation efficiency of the dipole above RIS with loss tangent $\tan\delta = 0.001$ at resonance is about $e_r = 89\%$, which is lower than the efficiency of antenna over RIS operating below resonance (RIS with moderate value of ν).

2) Patch Over RIS: Next we consider performance of a patch antenna over the RIS and compare its performance with

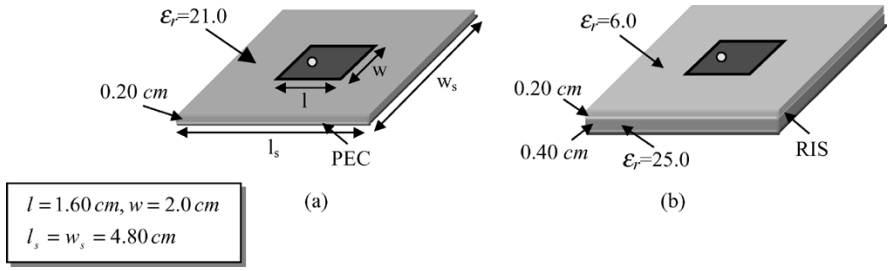

Fig. 18. Patch antenna on the (a) conventional substrate and (b) RIS substrate (a 4 × 4 array of square patches printed on the PEC-backed dielectric material).

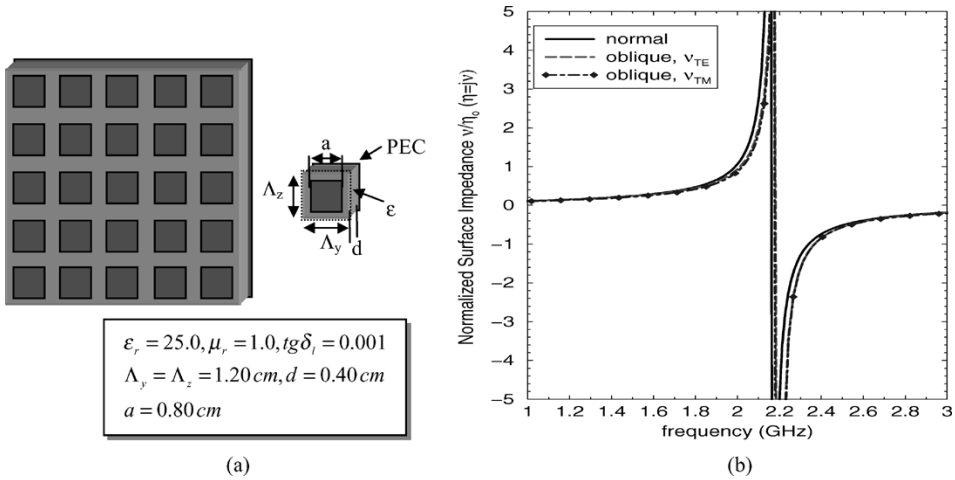

Fig. 19. (a) Periodic RIS substrate for the novel design of patch antenna and (b) surface impedance characteristics. Notice to the similar impedance behaviors for the normal and oblique incident plane waves.

a traditional patch over a PEC surface. As demonstrated in the previous example we expect that an inductive RIS will also miniaturize the size of a patch, which is capacitive below its natural resonance. To make the comparison with the conventional patch antennas relevant, we use the same size patch and ground plane; however, we allow the permittivity of the substrate of the conventional patch to be a variable to achieve the same resonant frequency.

Fig. 18(b) shows the geometry of a patch antenna printed on a relatively low dielectric material $\varepsilon_r = 6$ and located above an RIS. The geometry of periodic RIS substrate designed for patch antenna and its impedance performance are shown in Fig. 19. In order to increase the number of square RIS metallic patches on a relatively small size substrate (4.8 cm × 4.8 cm) a large dielectric material with $\varepsilon_r = 25.0$ is used for the design of RIS. Fig. 19(b) shows the spectral response of the RIS reactance at normal and oblique incidences. With a higher dielectric constant the variation of surface reactance with frequency is sharper than that of the RIS designed with $\varepsilon_r = 12.0$.

A patch antenna with a miniaturized size $\lambda_0/10$ is capable of efficient radiation above this RIS at $f_0 = 1.86$ GHz. As before simulation results are obtained from the FDTD code. Fig. 20 shows the return loss of this antenna demonstrating a very wide bandwidth of about $BW = 5.0\%$. To achieve the same resonant frequency (1.86 GHz), a conventional patch was designed on a high dielectric substrate $\varepsilon_r = 21.0$ whose geometry is shown in Fig. 18(a). The return loss of this antenna is also shown in Fig. 20 for comparison. The conventional patch antenna, over the $0.30\lambda_0 \times 0.30\lambda_0$ ground plane, shows a very narrow bandwidth of $BW = 0.63\%$ and an efficiency of about $e_r = 70\%$.

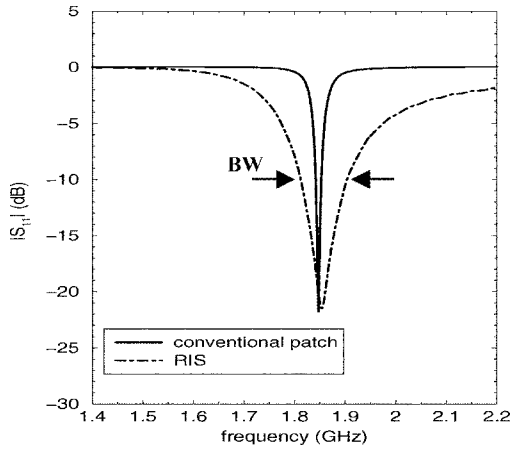

Fig. 20. Return loss of patch antenna over the conventional and RIS substrates. Notice to the wideband performance of the miniaturized patch on the RIS substrate.

The bandwidth of the same size patch and substrate antenna over RIS has a bandwidth eight times larger than the conventional patch antenna. Note that one may increase the thickness of conventional substrate to provide more bandwidth, however, this generates difficulty in antenna impedance matching and additionally still the less bandwidth compared to the RIS substrate is achieved.

The directivity and front-to-back ratio of the patch antenna on the RIS are calculated to be $D_0 = 4.95$ and 6 dB, respectively. The efficiency is around $e_r = 95\%$. The antenna cross polarization isolation is about -30 dB. The radiation patterns of both patch antennas are plotted in Fig. 21.

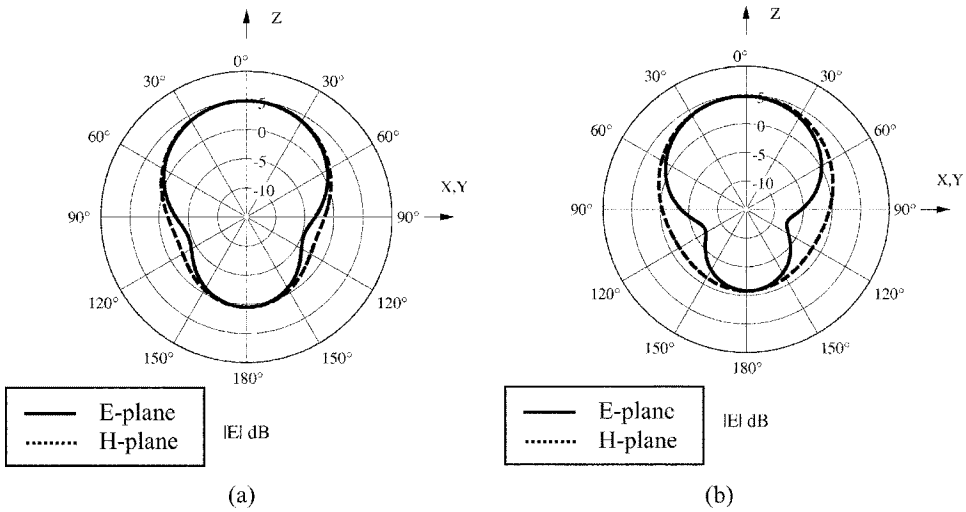

Fig. 21. Radiation patterns of patch antenna over the (a) conventional and (b) RIS substrates. Although, they have almost the same radiation patterns, however, the RIS provides the much higher gain/efficiency.

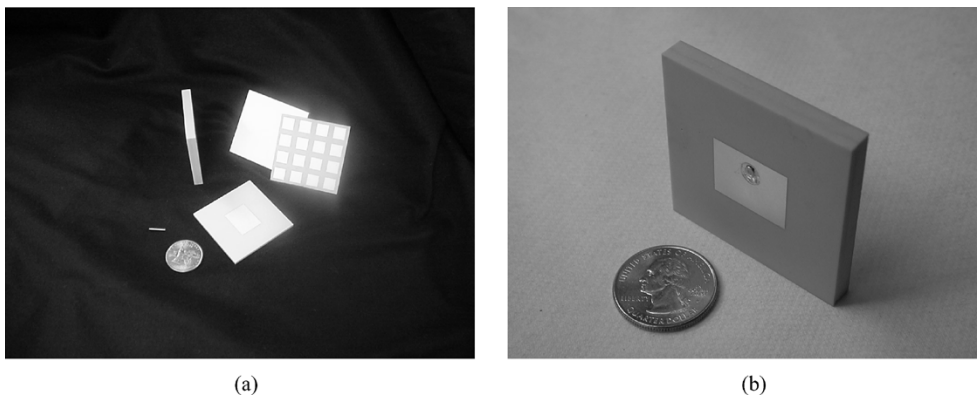

Fig. 22. Fabrication of patch on the RIS substrate. (a) Magnesium silicate and magnesium calcium titanate blocks metalized and etched. (b) Assembled patch antenna over the RIS substrate.

To verify these results experimentally, the design of the patch antenna on the RIS is fabricated and tested. Two independent layers are fabricated separately on high quality ceramic substrates. The dielectric material used for the patch antenna substrate is Trans-Tech D-6 magnesium silicate ($\varepsilon_r = 6$), commonly known as Forsterite. The RIS substrate is made using Trans-Tech MCT-25 magnesium calcium titanate composition ($\varepsilon_r = 25$). Using a thick film silver paste and Trans-Tech's screen printing process, the array of square patches, corresponding metal backing, and patch are generated. Both substrates are heat treated to form an intimate bond of the silver to the dielectric material. This intermediary stage is diagrammed in Fig. 22(a). Using a two-part, low loss dielectric adhesive, the substrates are assembled in a fixture to ensure alignment. The feed-hole is then drilled into the assembly. The feed-thru pin is machined from hardened brass and soldered to the silver patch. The completed antenna structure is shown in Fig. 22(b).

The return loss of the fabricated patch antenna is measured and plotted in Fig. 23(a). The antenna resonance is found to be at $f_0 = 1.92$ GHz and it exhibits an impedance match with better than -25 dB return loss. The measured relative bandwidth is $BW = 6.71\%$. The radiation patterns are measured in the anechoic chamber of the University of Michigan Radiation Laboratory and are shown in Fig. 23(b). The gain and front-to-back ratio are, respectively, measured to be $G = 4.5$ dBi and 5.6 dB. This measured gain corresponds to an excellent radiation efficiency of $e_r = 90\%$. To our knowledge this is the highest reported gain and bandwidth for such a small planar antenna.

V. Conclusion

In this paper a novel reactive impedance substrate for antenna miniaturization with enhanced bandwidth performance is introduced. Analytical, numerical, and experimental analyzes were carried out to demonstrate the basic concept, design procedure, and model verifications. Three properties of reactive impedance surfaces are utilized to achieve the desired antenna properties. These include: 1) total power reflection that creates the desired front-to-back ratio; 2) spatially distributed image representation that minimizes mutual coupling between the antenna and its image; and 3) the ability to store magnetic (or electric) energy that can compensate for the near-field electric (or magnetic) energy of the radiating structure. These last two properties allow for ease of impedance matching over a relatively wide bandwidth and antenna miniaturization. A practical approach for design and fabrication of RIS substrates is also presented. This surface is simply constructed from a periodic structure of square

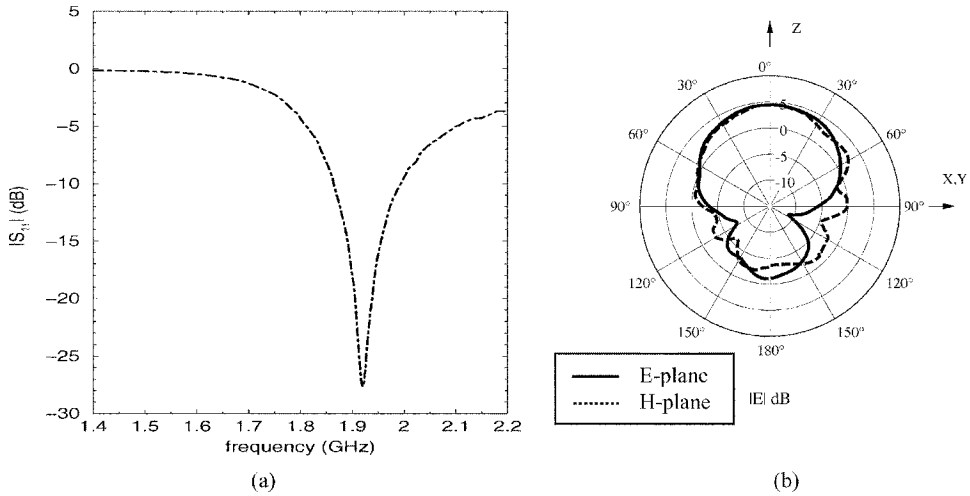

Fig. 23. Measured performance of patch antenna over the RIS substrate. (a) Return loss and (b) radiation patterns. There are good agreements between the measured and FDTD based results (Figs. 20 and 21).

patches printed on a PEC-backed dielectric material. An approximate circuit model and a full-wave FDTD numerical technique are developed for designing and characterizing reactive impedance surfaces. A miniaturized $\lambda_0/10$ patch antenna over an RIS substrate was fabricated and tested. It was shown that the antenna over RIS exhibits superior characteristics when compared to the conventional patch antenna. The measured relative bandwidth, antenna gain, and radiation efficiency of the RIS patch antenna are, respectively, $BW = 6.7\%$, $G = 4.5$ dBi, and $e_r = 90\%$. This constitutes the highest bandwidth, gain, and efficiency reported for such a small size thin planar antenna.

ACKNOWLEDGMENT

The authors would like to thank D. Cruickshank and C. Decker from Trans-Tech for fabricating the antenna, and K. Buell from the University of Michigan for performing the measurements.

REFERENCES

[1] N. G. Alexópoulos and D. R. Jackson, "Fundamental superstrate (cover) effects on printed circuit antennas," *IEEE Trans. Antennas Propagat.*, vol. AP32, pp. 807–816, Aug. 1984.

[2] D. R. Jackson and N. G. Alexópoulos, "Gain enhancement methods for printed circuit antennas," *IEEE Trans. Antennas Propagat.*, vol. 33, pp. 976–987, Sept. 1985.

[3] T. Ozdemir, P. Frantzis, K. Sabet, L. Katehi, K. Sarabandi, and J. Harvey, "Compact wireless antennas using a superstrate dielectric lens," in *Proc. IEEE AP-S Int. Symp.*, Salt Lake City, UT, July 16–21, 2000.

[4] R. K. Mongia and P. Bhartia, "Dielectric resonator antennas-A review and general design relations for resonant frequency and bandwidth," *Int. J. Microwave and Millimeter-Wave Computer-Aided Engineering*, vol. 4, no. 3, pp. 230–247, July 1994.

[5] A. Petosa, A. Ittipiboon, Y. M. M. Antar, D. Roscoe, and M. Cuhaci, "Recent advances in dielectric-resonator antenna technology," *IEEE Antennas Propagat. Mag.*, vol. 40, no. 3, pp. 35–48, June 1998.

[6] D. Sievenpiper, L. Zhang, R. F. J. Broas, N. G. Alexópoulos, and E. Yablonovitch, "High-impedance electromagnetic surfaces with a forbidden frequency band," *IEEE Trans. Microwave Theory Tech.*, vol. 47, pp. 2059–2074, Nov. 1999.

[7] J. Yeo and R. Mittra, "Bandwidth enhancement of multiband antennas using frequency selective surfaces for ground planes," in *Proc. IEEE AP-S Int. Symp.*, Boston, MA, July 8–13, 2001.

[8] I. V. Lindell and E. Alanen, "Exact image theory for the Sommerfeld half-space problem, Part I: Vertical magnetic dipole," *IEEE Trans. Antennas Propagat.*, vol. AP-32, pp. 126–133, Feb. 1984.

[9] ——, "Exact image theory for the Sommerfeld half-space problem, Part II: Vertical electric dipole," *IEEE Trans. Antennas Propagat.*, vol. AP-32, pp. 841–847, Aug. 1984.

[10] ——, "Exact image theory for the Sommerfeld half-space problem, Part III: General formulation," *IEEE Trans. Antennas Propagat.*, vol. AP-32, pp. 1027–1032, Oct. 1984.

[11] K. Sarabandi, "Scattering from variable resistive and impedance sheets," *J. Electromagn. Waves Applicat.*, vol. 4, no. 9, pp. 865–891, 1990.

[12] K. Sarabandi, M. D. Casciato, and I. S. Koh, "Efficient calculation of the fields of a dipole radiating above an impedance surface," *IEEE Trans. Antennas Propagat.*, vol. 50, pp. 1222–1235, Sept. 2002.

[13] A. Taflove and S. C. Hagness, *Computational Electrodynamics: The Finite-Difference Time-Domain Method*, Norwood, MA: Artech House, 1995.

[14] A. Taflove, *Advances in Computational Electrodynamics: The Finite-Difference Time-Domain Method*, Norwood, MA: Artech House, 1998.

[15] H. Mosallaei and Y. Rahmat-Samii, "Broadband characterization of complex periodic EBG structures: An FDTD/prony technique based on the split-field approach," *Electromagn. J.*, vol. 23, no. 2, pp. 135–151, Feb.-Mar. 2003.

[16] W. R. Smythe, *Static and Dynamic Electricity*. New York: McGraw-Hill, 1968.

[17] H. B. Dwight, *Tables of Integrals and other Mathematical Data*. New York: Macmillan, 1961.

Hossein Mosallaei (SM'98) received the B.Sc. and M.Sc. degrees in electrical engineering from Shiraz University, Shiraz, Iran, and the Ph.D. degree in electrical engineering from the University of California, Los Angeles (UCLA), in 1991, 1994, and 2001, respectively.

From 1995 to 1997, he was with the Electrical Engineering Department at Shiraz University. From 1997 to 2001, he was a Research Assistant and Teaching Associate at UCLA. Currently, he is is a Research Scientist in the Department of Electrical Engineering and Computer Science, University of Michigan-Ann Arbor. His research interests include meta-materials, smart RF/wireless systems, novel communication antennas, micro-electromagnetics, periodic structures, EBG and photonic crystals, high frequency circuits, bioengineering, and computational EM.

Dr. Mosallaei is a Member of the International Scientific Radio Union (URSI) Commission B. He was the recipient of student prize paper awards in AP-S 2000, '01, '03, a URSI Young Scientist Award in 2001, and RMTG award in 2002. He was the organizer of Radiation Laboratory seminars at the University of Michigan-Ann Arbor in 2002 and 2003. He has also served as Chairman and Co-Chairman of several national and international symposia. He is listed in *Who's Who in America*.

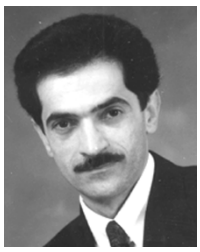

Kamal Sarabandi (S'87–M'90–SM'92–F'00) received the B.S. degree in electrical engineering from Sharif University of Technology, Tehran, Iran, in 1980, the M.S. degree in electrical engineering/mathematics, and the Ph.D. degree in electrical engineering from The University of Michigan-Ann Arbor, in 1986 and 1989, respectively.

He is Director of the Radiation Laboratory and a Professor in the Department of Electrical Engineering and Computer Science, The University of Michigan-Ann Arbor. He has 20 years of experience with wave propagation in random media, communication channel modeling, microwave sensors, and radar systems and is leading a large research group consisting of four research scientists, ten Ph.D. students, and two M.S. students. Over the past ten years he has graduated 15 Ph.D. students. He has served as the Principal Investigator on many projects sponsored by NASA, JPL, ARO, ONR, ARL, NSF, DARPA, and numerous industries. He has published many book chapters and more than 105 papers in refereed journals on electromagnetic scattering, random media modeling, wave propagation, antennas, microwave measurement techniques, radar calibration, inverse scattering problems, and microwave sensors. He has had more than 220 papers and invited presentations in national and international conferences and symposia on similar subjects. His research areas of interest include microwave and millimeter-wave radar remote sensing, electromagnetic wave propagation, and antenna miniaturization.

Dr. Sarabandi is a Member of the International Scientific Radio Union (URSI) Commission F and of The Electromagnetic Academy. He received the Henry Russel Award from the Regent of The University of Michigan-Ann Arbor (the highest honor the University of Michigan bestows on a faculty member at the assistant or associate level). He received a 1996 Teaching Excellence Award from the Department of Electrical Engineering and Computer Science and a 1999 GAAC Distinguished Lecturer Award from the German Federal Ministry for Education, Science, and Technology, given to about ten individuals worldwide in all areas of engineering, science, medicine, and law. He also received the 2003/2004 College of Engineering Research Excellence Award, The University of Michigan-Ann Arbor. In the past several years, joint papers presented by his students at a number of symposia (IEEE AP'95,'97,'00,'01,'03 IEEE IGARSS'99,'02, IEEE MTTS'01) have received student prize paper awards. He is a Vice President of the IEEE Geoscience and Remote Sensing Society (GRSS), a past Chairman of the Awards Committee of the IEEE GRSS from 1998 to 2002, and a Member of the IEEE Technical Activities Board Awards Committee from 2000 to 2002. He is an Associate Editor of the IEEE TRANSACTIONS ON ANTENNAS AND PROPAGATION and the IEEE SENSORS JOURNAL. He is listed in *American Men & Women of Science*, *Who's Who in America*, and *Who's Who in Electromagnetics.*